光学学报

空间光学模拟计算的发展与应用

刘勇良[1]，刘文玮[1]，程化[1*]，陈树琪[1,2,3**]

[1]南开大学物理科学学院，泰达应用物理研究院，弱光非线性光子学教育部重点实验室，天津 300071；

[2]南开大学材料科学与工程学院，智能传感交叉科学中心，天津 300350；

[3]山西大学极端光学协同创新中心，山西 太原 030006

摘要 空间光学模拟计算具有大规模并行计算、低功耗和超快响应速度的信息处理优势，在图像处理、边缘检测和机器学习方面显示出巨大的应用潜力。本文回顾了空间光学模拟计算的发展，着重阐述了空间光学模拟计算结合超表面在不同理论模型及体系中的研究进展与应用，通过引入人工微结构替代传统大尺寸光学元件，推动空间光学模拟计算器件向微型化、集成化发展；总结了基于自旋轨道耦合、拓扑等物理效应的新型空间光学模拟计算最新进展，为实现超带宽高速信息处理提供了新思路；对空间光学模拟计算现有挑战和研究前景进行了分析和讨论。

关键词 空间光学模拟计算；空间微分器；傅里叶光学；超表面；光学自旋霍尔效应

中图分类号 O436 **文献标志码** A **DOI**：10.3788/AOS231152

1 引 言

人工智能、自动驾驶、大数据等领域飞速发展所带来的海量数据对计算工具提出了更高的要求。近年来，随着超大规模集成电路的发展，电子计算机的体积不断缩小，数据处理速度也大幅度提升[1]。然而，由于电子器件逐步受到量子效应等物理极限的制约，数字计算电路低功耗、微型化的提升速度越来越慢。此外，传统模拟信号处理需要经过模/数转换、信号处理和数/模转换过程，不可避免的转换延迟以及电子器件的高功耗使得传统模拟计算不具备大规模信息并行处理的能力[2]。因此，研究人员致力于开发新型计算系统来弥补传统电子计算系统的诸多缺点，其中构建以光信号为信息载体的全光系统吸引了越来越多学者的关注[3]。光信号处理系统分为数字运算和模拟运算两种。光信号数字计算最早采用基于光电混合的液晶空间光调制器进行逻辑运算，而光学模拟计算不涉及光电转换，能够通过微分、积分运算等直接在时间和空间上操控光信号。时域模拟光学计算通常在时间频率域对输入光脉冲进行调制，以实现相应的时域模拟计算。在时域中，微分方程求解、模拟计算已被广泛应用于高速脉冲调制[4-8]。目前，时间光学模拟计算大致分为共振结构和非共振结构两类。在共振体系下，Kulishov等[9]采用长周期光纤光栅实现了时域一阶微分计算，Slavík等[10]利用光纤光栅结构在太赫兹波段实现了时域微分运算。在非共振体系下，Liu等[11]提出了可集成光学信号处理器，利用半导体光放大器、相位调制器等器件实现对光脉冲的时域微分运算。之后，研究人员又陆续设计了积分运算[12-13]、对数运算[14]、希尔伯特变换[15-17]等时域模拟器件。空间光学模拟计算的目标是获得所需的空间频谱传递函数。与时间域相比，光场空间域在振幅、相位等方面具有丰富的调控自由度，有利于空间三维并行计算，因而出现其独有的拉普拉斯、散度等模拟运算。光学传输的多种效应都对应于微积分运算，如光的反射、干涉、衍射等。同时，空间微分可直接用于图像边缘提取，进而在显微成像、图像增强、模式识别等新兴领域有广阔的应用前景。此外，通过光学方式也可以实现其他类型的计算，如加法运算、减法运算以及卷积运算。光学逻辑门和光学开关等器件也可以用于实现光学计算。通过将输入光信号与特定光学元件相互作用，可以实现与、或、非等逻辑运算。光学量子计算利用光子的量子特性进行计算。量子计算通过量子叠加和量子纠缠等现象，可以在某些特定问题上实现比传统计算机更高效的计算。基于Abbe成像理论，4*f*光学滤波系统得以诞生，并广泛用于空域光学模拟计算。该系统由傅里叶变换透镜、空间频率滤波器和傅里叶逆变换透镜组成。通过设计具有特定功能的空间滤波器，可以获得所需的输出空间光场，这

收稿日期：2023-06-18；**修回日期**：2023-07-23；**录用日期**：2023-07-28；**网络首发日期**：2023-07-31

基金项目：国家重点研发计划(2021YFA1400601，2022YFA1404501)、国家杰出青年科学基金(11925403)、国家自然科学基金(12122406，12192253，12274239，U22A20258)

通信作者：*hcheng@nankai.edu.cn；**schen@nankai.edu.cn

就是传统 4*f* 系统进行光学信息处理的关键。传统 4*f* 系统采用大尺寸光学元件进行光学信息处理，导致整个系统体积庞大，无法与现代微型化、集成化的信号处理器件兼容。最近，研究人员将光学模拟计算与人工微结构相结合，为空间光学模拟处理器的进一步集成化、微型化提供了可能。

人工微结构是一种人工设计的材料，其结构尺寸接近或小于波长。通过设计特定的结构单元，能够实现对入射光场的灵活调控，包括光的振幅、相位、偏振态等。目前，人工微结构已广泛用于透镜成像[18-20]、全息成像[21-22]、结构色[23]以及非线性调控器件[24-25]。随着纳米制造技术的不断发展创新，人们尝试设计特定的人工微结构来替代传统的大尺寸光学器件，推动空间光学模拟计算系统向微型化、集成化和低功耗发展[26-29]。2014 年，Silva 等[30]采用人工微结构实现了空间光学模拟计算器件。基于传统的 4*f* 空间滤波系统，研究人员利用两块梯度折射率（GRIN）透镜和超表面分别代替传统的傅里叶透镜和空间滤波器，通过优化特定人工微结构实现所需的空间光学模拟计算。与传统模拟计算相比，结合人工微结构的空间光学模拟计算器具有实时、低功耗和集成化的优点，已被广泛应用于信息处理[31-36]、成像[37-41]、求解方程[42-43]等领域。

空间光学模拟计算器件的设计原理可以分为等效介质理论、基于共振光学的原理以及基于非共振光学的原理，如图 1 所示。当超表面的结构尺寸远小于工作波长时，研究人员利用有效介电常数和磁导率描述非均匀介质材料。通过设计超表面的透射（反射）率空间分布，可以获得所需数学运算的空间频谱传递函数，但该方法需要引入空间傅里叶变换和傅里叶逆变换，器件整体尺寸较大。在共振体系下，共振的激发要求动量匹配，共振结构对入射光中不同方向的波矢分量具有不同的响应，使光场在结构中传播的空间响应频率符合特定的光学模拟计算。同时，该方法无需引入傅里叶变换，整个光学器件尺寸进一步缩小。典型的例子有基于表面等离激元（SPP）的空间模拟微分器和基于电偶极子共振的空间模拟微分器。对比共振式模拟运算器有限的空间带宽，在非共振体系的特定条件下，基于自旋霍尔效应、布儒斯特效应以及 Pancharatnam-Berry（PB）相位超表面，研究人员也能实现多种空间光学模拟计算。本文主要介绍近年来空间光学模拟计算的发展与应用，讨论了空间光学模拟计算的基本设计思路及其分类，阐述了不同空间模拟计算的设计原理、功能特点及研究进展，并总结了空间光学模拟计算未来的发展方向和应用场景。

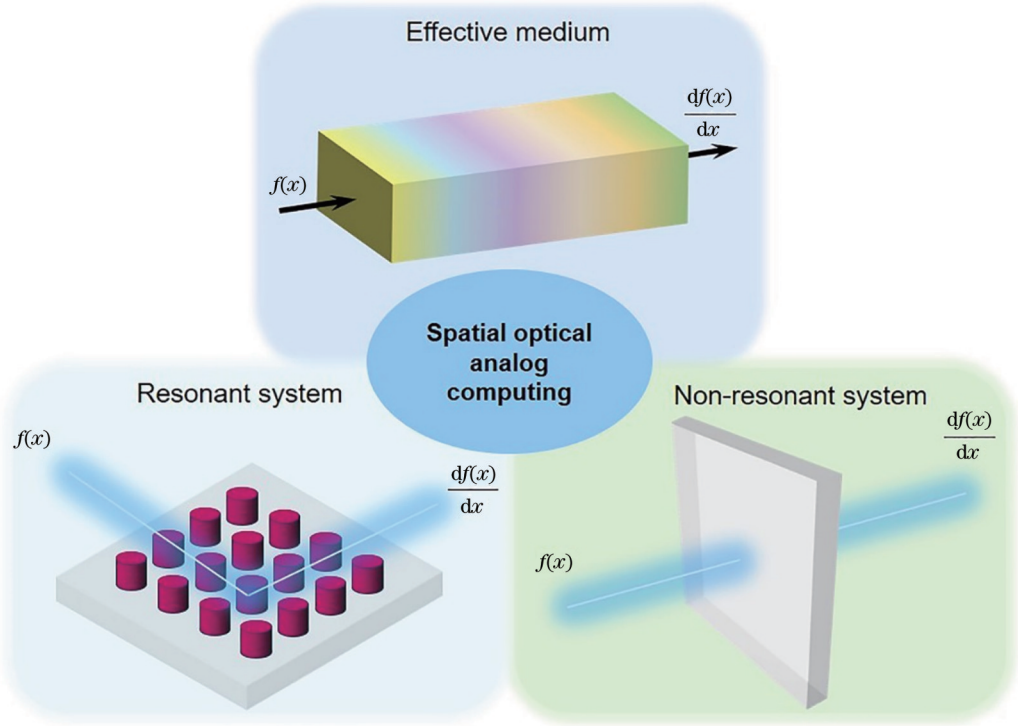

图 1　不同物理体系中的空间光学模拟计算

Fig. 1　Spatial optical analog computing in different physical systems

2　等效介质理论

为实现集成化、微型化的空间光学模拟计算系统，Silva 等[30]将超表面引入空间光学模拟计算器件，并提出了两种设计思路：傅里叶滤波法和格林函数法。傅里叶滤波法基于传统 4*f* 空域光学滤波系统。该方法利用两块格林透镜分别实现傅里叶变换和傅里叶逆变换。通过空间频谱面的超表面调控入射光场的空间频

谱分布，使器件的空间频谱传递函数满足空间模拟运算所需的形式。研究人员利用GRIN(+)、GRIN(−)透镜和超表面分别替代传统4f系统的透镜和空间频率滤波器，分别实现空间傅里叶变换、空间傅里叶逆变换以及光场空间频谱调控，从而进行空间光学模拟计算，如图2(a)所示。对于GRIN(+)透镜，其磁导率$\mu=\mu_0$，介电常数为$\varepsilon(y)=\varepsilon_c\left[1-\left(\pi/2L_g\right)^2y^2\right]$，其中$\varepsilon_c$为GRIN中心平面的介电常数，$L_g$为GRIN的特征长度。GRIN(−)透镜的磁导率和介电常数分别为$\mu=-\mu_0$和$\varepsilon=-\varepsilon(y)$。假设超表面对输入$f(y)$进行一阶微分运算，输出的$g(y)$应满足$g(y)\propto \mathrm{d}f(y)/\mathrm{d}y$，理想传递函数$\tilde{G}(y)\propto \mathrm{i}y/y_0$，其中$y_0=W/2$，$W$为超表面宽度。使用超表面取代传统空间滤波器，为减少反射，超表面的介电常数和磁导率满足$\varepsilon_{MS}(y)/\varepsilon_0=\mu_{MS}(y)/\mu_0$，其中$\varepsilon_0$和$\mu_0$分别为真空介电常数和磁导率，则

$$k=k_0\sqrt{\left[\varepsilon_{MS}(y)/\varepsilon_0\right]\left[\mu_{MS}(y)/\mu_0\right]}=k_0\varepsilon_{MS}(y)/\varepsilon_0,\quad(1)$$

式中：$k_0=2\pi/\lambda_0$，λ_0为自由空间工作波长。利用超表面实现输入$f(y)$的一阶微分运算，则超表面的相对介电常数和磁导率为

$$\frac{\varepsilon_{MS}(y)}{\varepsilon_0}=\frac{\mu_{MS}(y)}{\mu_0}=\mathrm{i}\left(\frac{\lambda_0}{2\pi\Delta}\right)\ln\left(\frac{-\mathrm{i}W}{2y}\right)。\quad(2)$$

假设波长$\lambda_0=3\ \mu\mathrm{m}$，$W\approx10\lambda_0$，$L_g\approx12\lambda_0$，$\varepsilon_c=2.01\varepsilon_0$，$\Delta=\lambda_0/3$，若输入函数满足$f(y)=ay\exp\left(-y^2/b\right)$，其中$a=2.1\lambda_0^{-1}$，$b=\lambda_0^2/0.9$，经该光学系统后输出函数分布为$f(y)$的一阶导数。该方法能够同时实现微分、积分和卷积等数学运算，为新型微纳系统的发展铺平了道路。此后，Zhang等[44]通过平面电介质孔结构，基于等效介质理论实现了片上求解常微分方程的操作。之后，Khavasi团队[45-46]利用石墨烯实现多种空间模拟运算。通过电压调控器件的电导率获得特定的空间折射率分布，从而实现空间微分和积分运算[45]。

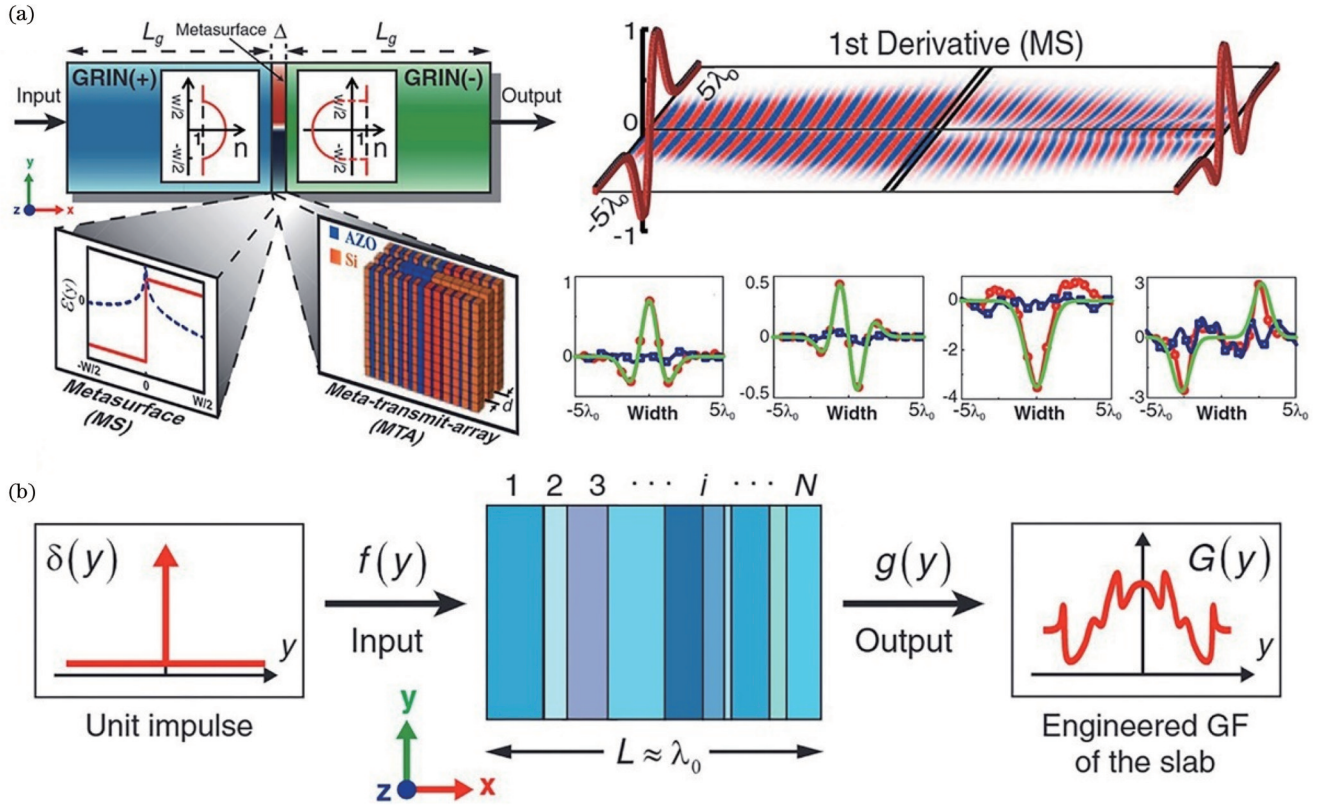

图2　等效介质理论空间光学模拟计算[30]。(a)基于GRIN透镜和超表面的多功能空间光学模拟计算；(b)基于多层介质膜的空间光学模拟计算

Fig. 2　Effective medium theory of spatial optical analog computing[30]. (a) Multifunctional spatial optical analog computing based on GRIN lenses and metasurfaces; (b) spatial optical analog computing based on multilayer dielectric film

与傅里叶滤波法不同，格林函数法直接在动量空间调制光信号，以实现空域模拟计算。相较于傅里叶滤波法，格林函数法仅需要单个微纳器件，无需格林透镜进行傅里叶变换，从而使得系统结构尺寸进一步缩小。为简化空间模拟计算系统，Silva等[30]通过设计横向均匀且纵向不均匀的多层超材料，实现所期望的脉冲响应，从而执行特定的数学运算，如图2(b)所示。假设输入函数为$f(y)$，为实现输出函数

$g(y)\propto\int f(y)\delta''(y-v)\mathrm{d}v$，结构的透射系数与波矢分量$k_y$的关系为$\tilde{G}(k_y)\propto -k_y^2$，通过优化结构的折射率、厚度等参数实现所需的空间频谱传递函数。由于多层平板结构横向对称，因此可以实现二阶导数运算$g(y)=\mathrm{d}^2f(y)/\mathrm{d}y^2$。该方法不仅可以有效地提高光计算系统的处理速度，还可以明显减小系统的体积。此后，研究人员利用多层薄膜结构实现多种空间模拟运算[47-50]。Doskolovich等[51]利用两种不同折射率薄膜交替堆叠，在30°入射角附近实现一阶微分运算。该课题组后续又利用类似多层介质膜结构，通过优化各层材料的组分和厚度参数实现多种数学运算，如拉普拉斯运算[52]、空间积分[53]以及时空模拟运算[54]。Wu等[55]采用硅和二氧化硅交替堆叠多层结构来实现反射式空间二阶微分运算，同时将神经网络与多层薄膜设计相结合，通过采用梯度下降法优化多层薄膜的反射系数来实现一阶、二阶微分运算[56]。该课题组还利用二氧化硅和二氧化钛堆叠的多层膜结构，实现了时域一阶微分和空域二阶微分运算[57]。Liu等[58]基于传输矩阵法设计氮化硅和二氧化硅薄膜交替堆叠的多功能平面光子芯片。在可见光波长下，无需改变结构参数即可实现一阶、二阶空间微分运算，获得入射光和透射光波函数之间的微分关系。相较于静态多功能微分器，Dai等[59]设计金属和水凝胶堆叠的多层薄膜来实现湿度敏感的可调空间微分运算。该设计能够在不同波长下交替实现明场成像或边缘增强，根据环境湿度主动调整模拟运算的工作波长。以上基于有效介质的理论研究，通过优化结构介电常数、磁导率和厚度等参数获得特定的传输系数，从而实现所需的空间模拟运算[60]。随着硅光子学技术逐渐成熟，Chen等[61]基于绝缘体硅(SOI)平台，利用两个超透镜和超表面实现片上空间光学积分器。通过调整SOI衬底上槽的宽度和长度，实现对传输幅值和相位的调控。通过优化超表面结构可以实现卷积、微分等运算。一方面，利用GRIN透镜、超表面替代传统4f系统的光学元件，使光学计算系统尺寸缩小至波长量级，但系统仍需傅里叶变换和固定焦距的自由空间进行光场传输，元件在系统频谱面上的位置需严格控制；另一方面，GRIN透镜、超表面和多层膜结构的设计和制备较为复杂。

3 共振式空间光学模拟计算

基于等效介质理论设计的器件结构复杂，实际制备难度较高大。同时，部分器件需要引入傅里叶变换等操作，器件的尺寸仍然较大。由于共振的激发要求动量匹配，共振结构通常对入射光中不同方向的波矢分量有不同的透射或反射[62-64]。基于共振原理的空间模拟计算无需傅里叶变换操作以及结构复杂的超表面，从而降低了实验难度，而且器件尺寸进一步压缩。基于SPP[65-70]、光栅[71-76]、光子晶体[77-79]等可以实现多种空间光学模拟计算。SPP是由电磁辐射与金属内的自由电子相互作用产生的。入射场与SPP耦合能够增强金属表面的电磁场，常用的激发方式有棱镜耦合、光栅耦合和波导耦合等。2014年，Ruan等[80]提出了用于描述金属-介质界面SPP的空间耦合膜理论，并通过激发金属-介质界面的SPP实现对空间光场的一阶微分运算[81]。同时引入增益介质，通过泵浦调控SPP的损耗率实现从空间微分到积分运算的转换。后续在临界耦合条件下，讨论了SPP对空间光场微分运算的处理速度和时间响应[82]。Zhang课题组[83]通过实验验证了基于SPP的空间一阶微分运算及图像边缘检测，如图3(a)所示。该设计由激发SPP的棱镜和单层银膜组成，利用特定角度的入射光激发金属银-介质界面上的SPP，在传播过程中泄漏辐射场与直接反射背景场干涉，在临界耦合条件下实现空间微分运算。该设计结构简单，但临界耦合条件需要获得较精确的参数数值。之后，Fang等[84]利用石墨烯-硅光栅结构在太赫兹波段实现空间二阶微分器。基于直接反射场和石墨烯表面两个反向传播的SPP泄漏波在输出端空间耦合干涉，在满足临界耦合条件后，反射输出光场为正入射输入光场的空间二阶微分，同时器件整体厚度小于工作波长的1/10。Lou等[85]将标量光场微分运算拓展到更为复杂的矢量光场运算，如图3(b)所示。通过激发石墨烯-硅结构SPP结合自旋霍尔效应，分别实现x与y方向的一阶微分运算。矢量光场使用波片校正x偏振和y偏振之间的相位差，当光经结构反射后再利用x方向偏振片检偏实现散度运算。Cordaro等[86]利用硅纳米束阵列超表面，基于Fabry-Pérot (FP)共振与准导模干涉获得不对称的Fano共振，实现空间二阶微分运算，如图3(c)所示。通过优化结构可以实现一阶微分运算，较大空间带宽和高效率的幅度曲线有利于其边缘成像分辨率接近衍射极限。2020年，Wan等[87]设计了硅纳米柱超表面，利用单元结构电偶极子共振的空间色散原理，对任意偏振光场进行空间二阶微分计算，并获得大空间带宽传递函数，如图3(d)所示。Komar等[88]利用硅纳米柱Mie共振的空间色散原理，在红外波段实现多通道二维空间微分运算和高分辨率边缘检测。利用介质光栅的导模共振，研究人员设计了多种空间模拟运算器。2014年，Golovastikov等[89]提出采用衍射光栅实现空间光学积分和微分运算。2015年，该课题组利用共振衍射光栅结合脉冲光场的时空傅里叶变换和严格耦合波理论，实现对脉冲光场时间二阶微分和空间一阶微分模拟运算[90]。Dantan课题组[91]提出通过固定氮化硅光栅结构同时实现空间一阶和二阶微分运算。该课题组通过入射角打破结构空间对称性，实现空间一阶微分运算。Fang等[92]设计了硅-二氧化硅-金衍射光栅结构，基于光栅背景衍射场与波导模式在输出端的耦合干涉，在近红外4个波

长处实现空间一阶微分运算。通过优化结构使其0级衍射输入光场经光栅微分运算后对应于1级衍射端口输出，其衍射效率能达到100%，并且输出端不同波长的光束能够自动解复用。Lou等[93]利用等离激元金属光栅实现空间微分器。此后，Rajabalipanah等[94]通过设计全金属超构光栅来调制输入信号的空间和角度特性，利用高阶空间谐波并行实现对称和非对称空间微分运算。Xu等[95]设计了双层等离子体光栅来实现光学时空微分器，该设计通过两层光栅结构来打破水平和垂直对称性，激发单向SPP，从而实现时间和空间一阶微分运算。Bezus等[96]设计了新颖的介质脊状结构，通过激发波导模式，当TE偏振斜入射时，在反射和透射端分别实现一阶空间积分和微分运算。同时，该结构中存在连续体束缚态，从而可以获得超高Q值。Guo等[97]提出一种采用光子晶体实现空间模拟运算的方案。该设计利用Γ点附近各向同性能带的C_{4v}旋转对称光子晶体结构，基于光子晶体板的导模共振，实现具有偏振不敏感的拉普拉斯运算及图像边缘成像。但工作空间带宽极小，其数值孔径约为0.01。此后，该课题组利用类似的光子晶体结构实现高通、低通等多功能滤波与图像处理[98]。Pan等[99]利用光子晶体在p偏振入射下实现二维拉普拉斯运算，如图3(e)所示。在Γ点存在无法被外部垂直入射平面波激发的对称保护型BIC，远离Γ点处准连续体束缚态(quasi-BIC)可以与入射平面波发生部分耦合。在一定范围内，通过增大入射角，quasi-BIC逐渐被激发，透射率增加。窄带宽的quasi-BIC以接近20°角入射，能够实现更好的边缘检测。此后，Zhou等[100]利用相似原理设计光子晶体来实现拉普拉斯运算，其对应的数值孔径为0.315，并能够与多种传统显微成像系统集成。

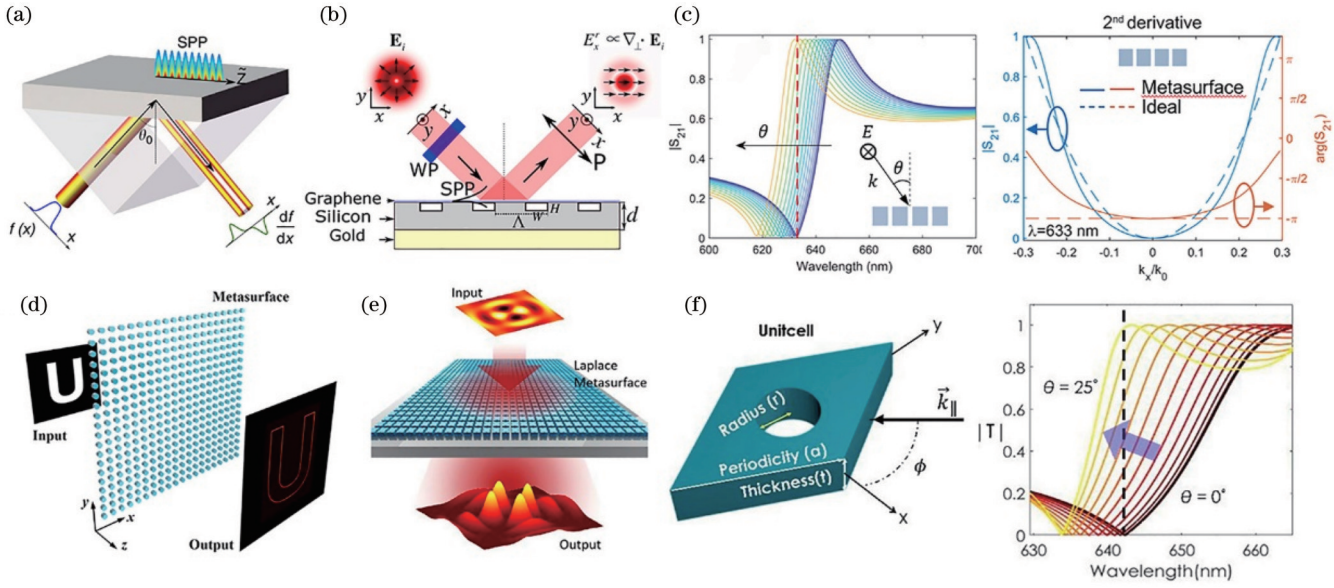

图3　共振体系空间光学模拟计算。(a) SPP共振空间微分[83]；(b)基于石墨烯超表面的矢量场散度运算[85]；(c)基于Fano共振的多功能微分器[86]；(d)电偶极子共振空间微分[87]；(e)基于光子晶体的准BIC拉普拉斯运算[99]；(f)非局域超表面多功能微分器[105]

Fig. 3　Resonant system of spatial optical analog computing. (a) Spatial differentiation based on SPP[83]; (b) divergence operation of vector fields based on graphene metasurface[85]; (c) Fano resonance enabled multifunctional differentiator[86]; (d) spatial differentiation based on electric dipole resonance[87]; (e) photonic crystal for Laplacian operation based on quasi-BIC[99]; (f) multifunctional differentiator with nonlocal metasurface[105]

相较于局域超表面，新兴的非局域超表面具有增强光和物质相互作用的优势[101]。由于非局域超表面的响应可以跨越多个单元，因此可以实现更为复杂的电磁波传输和辐射效应。通过改变入射角度，非局域超表面单元之间的相互作用和电磁响应也会发生变化。这种变化可能导致谐振频率随着入射角度的变化而发生改变，从而影响电磁波的传播方式[102-104]。Kwon团队[105]利用介质挖孔结构在横向空间频谱中引发非局域效应，如图3(f)所示。研究人员通过优化结构实现空间一阶、二阶微分运算以及2D图像边缘检测。上述共振结构通常对入射光束中不同方向的波矢分量有不同的反射率或透射率，因此无需傅里叶变换透镜即可实现对空间光场的模拟运算。

4　非共振式空间光学模拟计算

基于共振结构的空间模拟计算器件由于依赖共振，通常具有有限的空间带宽。近期，在非共振体系下，研究人员还实现了多种空间光学模拟计算。该方法的优点是对工作波长无特别选择，无需对结构的材料折射率、尺寸等进行特殊设计，简化了器件设计和实验制备过程。最近，研究者利用单个平行光学界面实现空间模拟运算[106-110]。2016年，Khavasi团队[111]利用

在空气-介质表面反射的布儒斯特角效应实现一阶微分运算，如图 4(a)所示。当横磁波的入射角满足布儒斯特定律时，其对应的反射率为 0，反射相位产生 π 跳变，该特点符合一阶微分运算条件。同时，反射系数可在布儒斯特角附近关于切向波矢进行一阶泰勒展开，只保留波矢一阶项近似时，传递函数为空间一阶微分函数。2020 年，Xu 课题组[112]在实验中利用单层玻璃基于布儒斯特效应实现二维空间光场的全方向导数运算。该课题组还利用棱镜基于古斯-汉森效应实现光学微分和图像边缘检测[113]，如图 4(b)所示。基于古斯-汉森效应实现边缘检测的空间分辨率由其位移决定。光束在棱镜内全反射，其古斯-汉森位移随入射角增大而减小，因此可以通过调整入射角来实现可调分辨率的边缘成像。Zhu 等[114]利用斜入射光在平行界面反射的光自旋霍尔效应实现空间一阶微分运算，如图 4(c)所示。斜入射线偏振光入射到光学平板界面中，出射光束的左、右旋分量发生相反的横向位移，若横向位移足够小，在自旋分量重叠区域插入与入射偏振正交的检偏器即可实现空间微分运算。He 等[115]采用倾斜偏振片，基于在介质界面的自旋霍尔效应在宽波段实现透射一阶微分运算。该课题组还验证了相位梯度可以通过微分运算转换为强度对比图像，利用玻璃界面的光自旋霍尔效应对相位分布进行微分操作[116]。为改善基于光自旋霍尔效应实现边缘检测对比度低的问题，Ji 等[117]分析了基于不同色散关系的单轴晶体对空间微分的影响。上述研究基于自旋霍尔效应引入垂直入射面位移来实现横向微分运算，而引入径向古斯-汉森效应能够实现运算方向的可调性。Zhu 等[118]将光的自旋霍尔效应和古斯-汉森效应结合，实现了方向、偏置可调的微分运算，并将其应用于相位物体的微分相衬成像和相位恢复。此后，该课题组将拓扑光学与空间模拟运算结合，在全内反射和布儒斯特角体系下提出具有非零拓扑荷数的传递函数，实现了各向同性二维微分运算[119]，如图 4(d)所示。光场在介质中全反射时，通过选取特定输出光场的偏振态，空间传递函数可设计为两个正交方向波矢的线性叠加，同时存在相位差。因此该设计类似于螺旋相位滤波片，光场通过器件后具 ±1 的拓扑荷数，同时微分器具有较好的鲁棒性和较大的光谱带宽。Song 等[120]利用各向异性晶体基于自旋轨道耦合实现透射式拓扑微分运算，如图 4(e)所示。由于自旋轨道相互作用，入射光的两个圆偏振分量被转换成具有相反拓扑荷数的光学涡旋，其产生的交叉极化场近似于入射光场的二阶微分运算结果。当满足特定条件时，入射光场在由两个不同折射率介质组成界面的反射或透射系数近似满足空间模拟运算。PB 相位超表面也能实现空间光学微分运

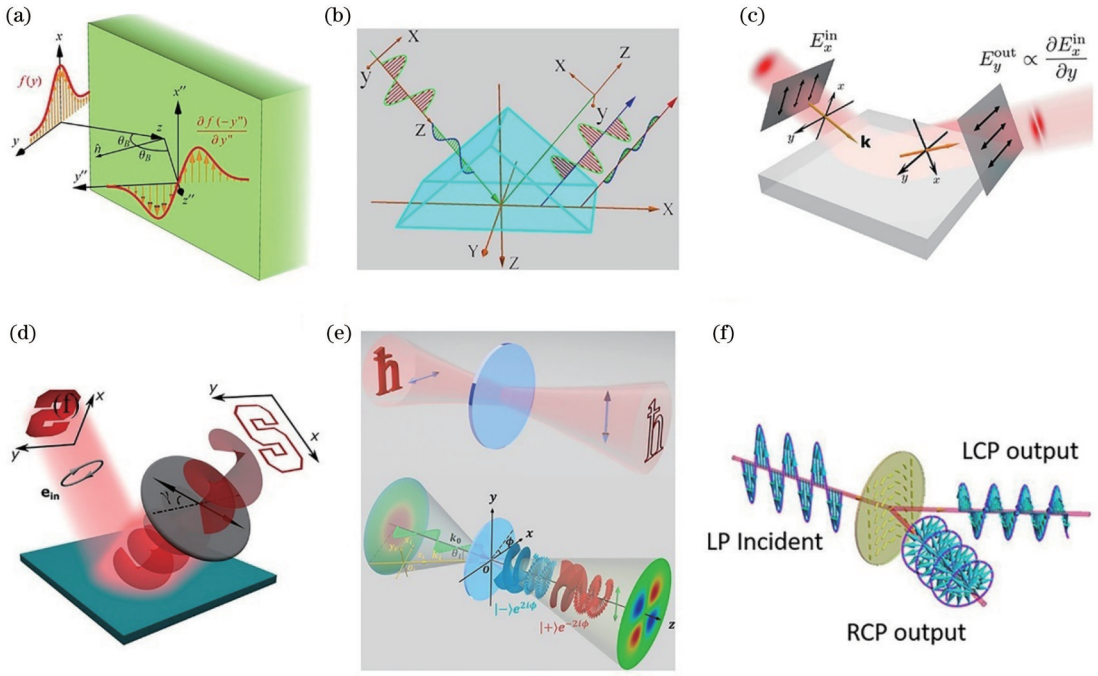

图 4　非共振空间光学模拟计算。(a)布儒斯特效应一阶微分运算[111]；(b)基于古斯-汉森效应的微分运算[113]；(c)基于光学自旋霍尔效应的空间微分运算[114]；(d)基于拓扑效应的微分运算[119]；(e)基于自旋轨道耦合的拓扑微分运算[120]；(f)基于 PB 相位超表面的空间微分运算[126]

Fig. 4　Non-resonant system of spatial optical analog computing. (a) First-order differentiation operation by Brewster effect[111]; (b) differentiation operation based on Goos-Hänchen effect[113]; (c) spatial differentiation operation from the spin Hall effect of light[114]; (d) differentiation operation based on topological effect[119]; (e) topological differentiation operation based on spin-orbit coupling[120]; (f) spatial differentiation based on PB phase metasurface[126]

算[121-124]。Xu 等[125]通过反向设计 PB 相位超表面实现模拟运算和全光图像边缘检测。基于庞加莱球面 PB 相位与超表面相应光轴之间的关系，通过调节 PB 相位超表面的光轴结构实现不同的光学微分操作。Zhou 等[126]将 PB 相位超表面插到两个正交排列的线性偏振元件之间，基于自旋-轨道耦合作用实现空间一阶微分运算，如图 4(f)所示。当线偏振光入射到 PB 相位超表面时，输出端获得具有相反位移方向的 LCP 和 RCP 两种光束分量。当 x 方向的线偏振光照射某物体时，其电场分布为 $\boldsymbol{E}_{\text{in}}(x,y)$。如果在傅里叶平面上引入设计的 PB 相位超表面，则对应的图像平面上的输出电场为

$$\boldsymbol{E}_{\text{out}}(x,y)=\boldsymbol{E}_{\text{in}}[(x-\Delta),y]\begin{pmatrix}1\\-\mathrm{i}\end{pmatrix}+\boldsymbol{E}_{\text{in}}[(x+\Delta),y]\begin{pmatrix}1\\\mathrm{i}\end{pmatrix},\tag{3}$$

式中：$\Delta=\frac{\lambda f}{\Lambda}$ 为 LCP 和 RCP 相反位移，其中 Λ 为超表面周期。该输出电场经过沿 y 方向的正交线性偏振器后，最终的输出电场为

$$\boldsymbol{E}_{\text{out}}(x,y)=\left\{\boldsymbol{E}_{\text{in}}[(x+\Delta),y]-\boldsymbol{E}_{\text{in}}[(x-\Delta),y]\right\}\begin{pmatrix}0\\\mathrm{i}\end{pmatrix}。\tag{4}$$

若位移 Δ 远小于图像轮廓，则 $\boldsymbol{E}_{\text{out}}(x,y)$ 为 $\boldsymbol{E}_{\text{in}}(x,y)$ 近似一阶空间微分

$$\boldsymbol{E}_{\text{out}}(x,y)\approx 2\Delta\frac{\mathrm{d}\boldsymbol{E}_{\text{in}}(x,y)}{\mathrm{d}x}。\tag{5}$$

此后，Zong 等[127]基于自旋霍尔效应，利用全介质超表面在可见光波段实现二维偏振不敏感的空间微分运算，其微分器的空间分辨率可达 1.7 μm。上述工作无需共振结构或设计复杂的超表面，但需借助额外偏振元件对入射、出射光束的偏振进行严格控制。

5 空间光学模拟计算相关应用

以光为信息载体，结合光场传播、干涉等物理过程的并行性，空间光学模拟计算能够实现超高速、大通量、低功耗的信息处理，其中空间微分、卷积运算可直接用于图像边缘检测。目前，光学图像处理方法主要有离散化数字处理、混合光电处理和全光学处理三类，其中光学图像处理方法能够避免电路功耗和速度影响，实现低功耗、超高速的图像处理[128]。由于大多数生物样品是透明的，染色观察会影响细胞的活性，将涡旋相位加载到傅里叶平面上可以实现相位物体的边缘提取。Kim 等[129]设计出一种将螺旋相位和双曲相位叠加的单层螺旋超透镜，该螺旋超透镜同时具有沿径向和切线方向的相位梯度，通过将低空间频率分量重新分布到较高的空间频率区域实现宽波段光学模拟计算与红细胞的边缘增强，如图 5(a)所示。Zhou 等[130]设计了一种几何相位介质超表面，在整个可见光波段实现二维空间微分和高对比度成像，并对生物细胞在明场、相差、暗场和边缘检测技术下的成像效果进行对比，结果如图 5(b)所示。与暗场和相差技术相比，该超表面与传统显微镜系统结合在细胞边缘检测中呈现出更为清晰的信号。针对传统全光卷积方法集成度低或功能单一的缺点，Fu 等[131]设计出单个超透镜和复振幅调制器来实现点扩散函数的修正，进而实现并行、实时的任意核全光卷积系统，如图 5(c)所示。该紧凑系统由实现傅里叶变换的超透镜与复振幅调制的超表面两部分组成。针对传统螺旋相位对显微镜边缘检测精度不可控的问题，该系统利用超表面引入额外的振幅调制，通过设计合适的卷积算子像素数的大小来控制检测精度。光学系统的点扩散函数由系统的孔径函数与调制器的傅里叶变换函数之间的卷积获得，通过超表面设计期望的复振幅调制器，对相位和振幅进行同时调控，实现边缘检测、空间微分、去噪和边缘增强操作，并对光学图像以及生物细胞进行图像处理。Wesemann 等[132]在玻璃封面上集成超构光栅作为增强盖玻片，利用纳米尺度的调控能力提高相位成像的对比度、分辨率，将纳米光子学与传统相位成像技术结合，为生物学相位成像提供全新思路，如图 5(d)所示。Zhang 等[133]利用介质超表面同时实现螺旋相差和明场成像，如图 5(e)所示。将螺旋相位和恒定相位分别与抛物线聚焦相位叠加到同一超表面，获得螺旋透镜相位和聚焦透镜相位；再分别引入偏转相位使两种成像空间分离，从而在同一视场内同步实现螺旋相差成像和明场成像。

6 总结和展望

空间光学模拟计算具有速度快、功耗低、带宽大等优势，在图像处理、边缘检测和机器学习方面显示出巨大的应用潜力。本文首先回顾了基于等效介质理论与共振式超表面空间光学模拟计算的发展，对近期空间光学模拟计算进行了分类。超表面取代传统空间滤波器实现特定的空间光学模拟计算，推动了空间模拟运算器向微型化、集成化发展。对比共振体系模拟计算的带宽等限制，介绍了基于布儒斯特角、光学自旋霍尔效应和光学拓扑等物理机制实现超宽带空间光学模拟计算的研究进展。最后，简要介绍了基于超表面的空间光学模拟计算在图像处理等方面的应用。

空间光学模拟计算结合超表面已经取得了前所未有的进步，但在超表面的制备技术、光学模拟计算的能量效率和计算复杂度等方面仍然面临着挑战。要想真正推动超表面走向实际应用，高精度、大面积、低成本的制备技术是关键。未来，结合超表面的新型空间模拟运算会出现更多全新方法，如尝试将图像低频部分通过散射等方式转为高频部分，打破能量效率和分辨率之间的权衡效应，并提高输出信号强度。同时推动空间光学模拟计算从简单到复杂发展，如简单模拟运

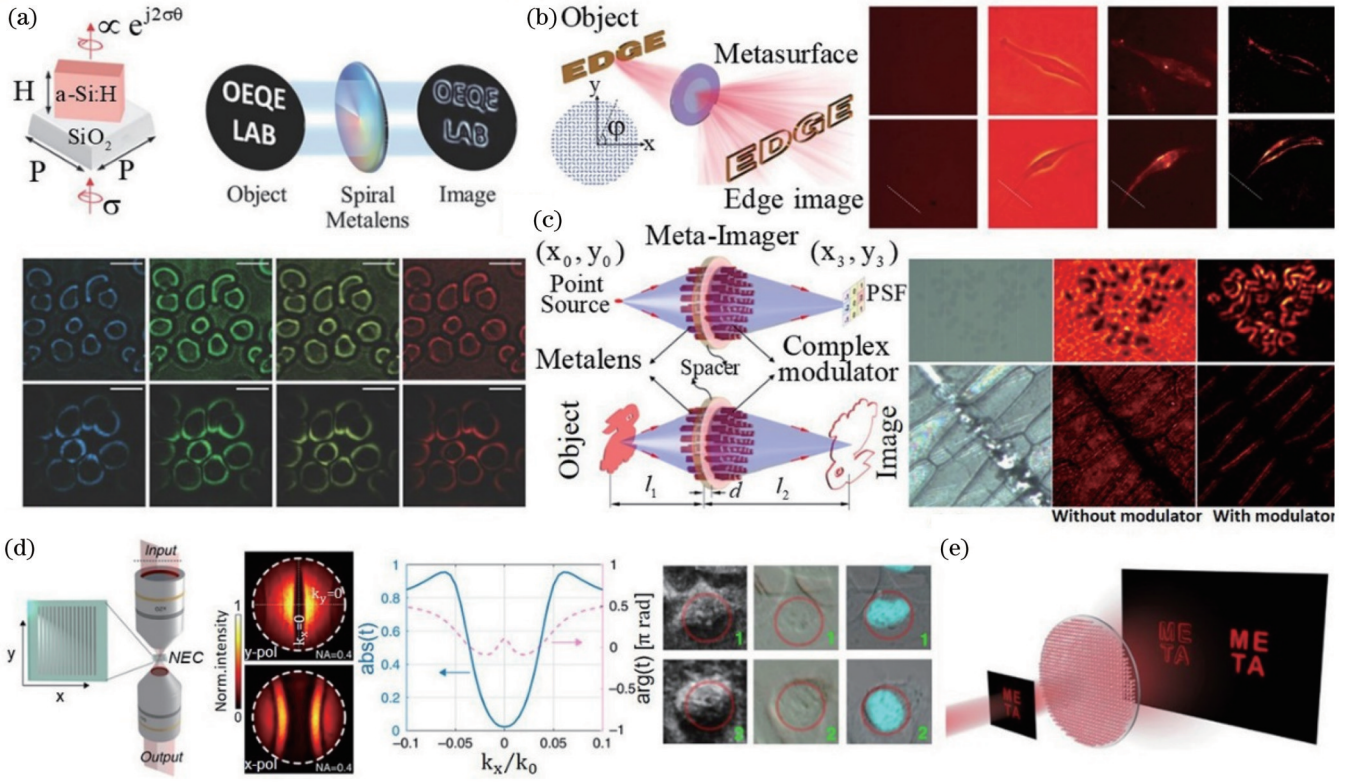

图 5　空间光学模拟计算应用。(a)基于螺旋超透镜的边缘增强[129];(b)基于 PB 相位超表面的高对比度成像[130];(c)基于超表面的任意全光卷积[131];(d)基于超构光栅的微分干涉对比显微镜[132];(e)基于超表面的多功能同步成像显微镜[133]

Fig. 5　Applications of spatial optical analog computing. (a) Spiral metalens for edge enhanced[129]; (b) high-contrast imaging based on PB phase metasurface[130]; (c) arbitrary all-optical convolution based on metasurface[131]; (d) differential interference contrast microscopy based on metagratings[132]; (e) multifunctional synchronous imaging microscope based on metasurface[133]

算向多通道复杂模拟运算发展,被动线性运算向可调控非线性模拟运算发展,直角坐标系中的模拟运算向极坐标系中的径向、角向模拟运算发展。随着技术的不断创新发展,由多种运算器件组合成的多功能光学运算芯片,有望在大通量光学通信、光学成像等领域发挥更加重要的作用。

参　考　文　献

[1] Hansson S O. Technology and mathematics[J]. Philosophy & Technology, 2020, 33(1): 117-139.

[2] Zangeneh-Nejad F, Sounas D L, Alù A, et al. Analogue computing with metamaterials[J]. Nature Reviews Materials, 2021, 6(3): 207-225.

[3] Huang Y D. Twenty years of photonics[J]. ACS Photonics, 2021, 8(2): 384-385.

[4] Tahmasebi O, Abdolali A, Rajabalipanah H, et al. Parallel temporal signal processing enabled by polarization-multiplexed programmable THz metasurfaces[J]. Optics Express, 2022, 30(25): 45221-45232.

[5] Sol J, Smith D R, del Hougne P. Meta-programmable analog differentiator[J]. Nature Communications, 2022, 13: 1713.

[6] Karimi A, Zarifkar A, Miri M. Design of ultracompact tunable fractional-order temporal differentiators based on hybrid-plasmonic phase-shifted Bragg gratings[J]. Applied Optics, 2018, 57(25): 7402-7409.

[7] Yang T, Dong J J, Lu L J, et al. All-optical differential equation solver with constant-coefficient tunable based on a single microring resonator[J]. Scientific Reports, 2014, 4: 5581.

[8] Wu J Y, Cao P, Hu X F, et al. Compact tunable silicon photonic differential-equation solver for general linear time-invariant systems[J]. Optics Express, 2014, 22(21): 26254-26264.

[9] Kulishov M, Azaña J. Long-period fiber gratings as ultrafast optical differentiators[J]. Optics Letters, 2005, 30(20): 2700-2702.

[10] Slavík R, Park Y, Kulishov M, et al. Terahertz-bandwidth high-order temporal differentiators based on phase-shifted long-period fiber gratings[J]. Optics Letters, 2009, 34(20): 3116-3118.

[11] Liu W L, Li M, Guzzon R S, et al. A fully reconfigurable photonic integrated signal processor[J]. Nature Photonics, 2016, 10(3): 190-195.

[12] Park Y, Ahn T J, Dai Y T, et al. All-optical temporal integration of ultrafast pulse waveforms[J]. Optics Express, 2008, 16(22): 17817-17825.

[13] Slavík R, Park Y, Ayotte N, et al. Photonic temporal integrator for all-optical computing[J]. Optics Express, 2008, 16(22): 18202-18214.

[14] Jiang Y S, DeVore P T S, Jalali B. Analog optical computing primitives in silicon photonics[J]. Optics Letters, 2016, 41(6): 1273-1276.

[15] Huang T L, Zheng A L, Dong J J, et al. Terahertz-bandwidth photonic temporal differentiator based on a silicon-on-isolator directional coupler[J]. Optics Letters, 2015, 40(23): 5614-5617.

[16] Ngo N Q, Song Y F. On the interrelations between an optical differentiator and an optical Hilbert transformer[J]. Optics Letters, 2011, 36(6): 915-917.

[17] Ashrafi R, Azaña J. Terahertz bandwidth all-optical Hilbert transformers based on long-period gratings[J]. Optics Letters, 2012, 37(13): 2604-2606.

[18] Wang Y J, Chen Q M, Yang W H, et al. High-efficiency broadband achromatic metalens for near-IR biological imaging window[J]. Nature Communications, 2021, 12: 5560.
[19] Liu W W, Li Z C, Li Z, et al. Energy-tailorable spin-selective multifunctional metasurfaces with full Fourier components[J]. Advanced Materials, 2019, 31(32): 1901729.
[20] Wang S M, Wu P C, Su V C, et al. A broadband achromatic metalens in the visible[J]. Nature Nanotechnology, 2018, 13(3): 227-232.
[21] Graydon O. Efficient holograms[J]. Nature Photonics, 2017, 11(2): 76.
[22] Wan W W, Gao J, Yang X D. Full-color plasmonic metasurface holograms[J]. ACS Nano, 2016, 10(12): 10671-10680.
[23] Yang B, Ma D N, Liu W W, et al. Deep-learning-based colorimetric polarization-angle detection with metasurfaces[J]. Optica, 2022, 9(2): 217-220.
[24] Li G X, Zhang S, Zentgraf T. Nonlinear photonic metasurfaces [J]. Nature Reviews Materials, 2017, 2: 17010.
[25] Jiang Y F, Liu W W, Li Z C, et al. Linear and nonlinear optical field manipulations with multifunctional chiral coding metasurfaces[J]. Advanced Optical Materials, 2023, 11(6): 2202186.
[26] Cordaro A, Edwards B, Nikkhah V, et al. Solving integral equations in free space with inverse-designed ultrathin optical metagratings[J]. Nature Nanotechnology, 2023, 18(4): 365-372.
[27] Babaee A, Momeni A, Abdolali A, et al. Parallel analog computing based on a 2×2 multiple-input multiple-output metasurface processor with asymmetric response[J]. Physical Review Applied, 2021, 15(4): 044015.
[28] Momeni A, Rajabalipanah H, Rahmanzadeh M, et al. Reciprocal metasurfaces for on-axis reflective optical computing [J]. IEEE Transactions on Antennas and Propagation, 2021, 69(11): 7709-7719.
[29] Momeni A, Safari M, Abdolali A, et al. Asymmetric metal-dielectric metacylinders and their potential applications from engineering scattering patterns to spatial optical signal processing [J]. Physical Review Applied, 2021, 15(3): 034010.
[30] Silva A, Monticone F, Castaldi G, et al. Performing mathematical operations with metamaterials[J]. Science, 2014, 343(6167): 160-163.
[31] Zhang J H, Chen S Q, Wang D, et al. Analog optical deconvolution computing for wavefront coding based on nanoantennas metasurfaces[J]. Optics Express, 2021, 29(20): 32196-32207.
[32] Wang Z, Li T T, Soman A, et al. On-chip wavefront shaping with dielectric metasurface[J]. Nature Communications, 2019, 10(1): 3547.
[33] Kashapov A I, Doskolovich L L, Bezus E A, et al. Spatial differentiation of optical beams using a resonant metal-dielectric-metal structure[J]. Journal of Optics, 2021, 23(2): 023501.
[34] Momeni A, Rajabalipanah H, Abdolali A, et al. Generalized optical signal processing based on multioperator metasurfaces synthesized by susceptibility tensors[J]. Physical Review Applied, 2019, 11(6): 064042.
[35] Rajabalipanah H, Abdolali A, Iqbal S, et al. Analog signal processing through space-time digital metasurfaces[J]. Nanophotonics, 2021, 10(6): 1753-1764.
[36] Moeini M M, Sounas D L. Discrete space optical signal processing[J]. Optica, 2020, 7(10): 1325-1331.
[37] Sulejman S B, Priscilla N, Wesemann L, et al. Thin film Notch filters as platforms for biological image processing[J]. Scientific Reports, 2023, 13: 4494.
[38] Zhou J X, Zhao J X, Wu Q Y, et al. Nonlinear computational edge detection metalens[J]. Advanced Functional Materials, 2022, 32(34): 2204734.
[39] Wang X W, Wang H, Wang J L, et al. Single-shot isotropic differential interference contrast microscopy[J]. Nature Communications, 2023, 14: 2063.
[40] Intaravanne Y, Ansari M A, Ahmed H, et al. Metasurface-enabled 3-in-1 microscopy[J]. ACS Photonics, 2023, 10(2): 544-551.
[41] He S S, Wang R S, Luo H L. Computing metasurfaces for all-optical image processing: a brief review[J]. Nanophotonics, 2022, 11(6): 1083-1108.
[42] Abdolali A, Momeni A, Rajabalipanah H, et al. Parallel integro-differential equation solving via multi-channel reciprocal bianisotropic metasurface augmented by normal susceptibilities [J]. New Journal of Physics, 2019, 21(11): 113048.
[43] Mohammadi Estakhri N, Edwards B, Engheta N. Inverse-designed metastructures that solve equations[J]. Science, 2019, 363(6433): 1333-1338.
[44] Zhang W X, Qu C, Zhang X D. Solving constant-coefficient differential equations with dielectric metamaterials[J]. Journal of Optics, 2016, 18(7): 075102.
[45] Abdollah-Ramezani S, Arik K, Khavasi A, et al. Analog computing using graphene-based metalines[J]. Optics Letters, 2015, 40(22): 5239-5242.
[46] Zangeneh-Nejad F, Khavasi A. Spatial integration by a dielectric slab and its planar graphene-based counterpart[J]. Optics Letters, 2017, 42(10): 1954-1957.
[47] Jin C Q, Yang Y M. Transmissive nonlocal multilayer thin film optical filter for image differentiation[J]. Nanophotonics, 2021, 10(13): 3519-3525.
[48] Momeni A, Rouhi K, Fleury R. Switchable and simultaneous spatiotemporal analog computing with computational graphene-based multilayers[J]. Carbon, 2022, 186: 599-611.
[49] Monticone F, Alù A, Galdi V, et al. "Computing metasurfaces" to perform mathematical operations[C]//2014 IEEE Antennas and Propagation Society International Symposium (APSURSI), July 6-11, 2014, Memphis, TN, USA. New York: IEEE Press, 2014: 27-28.
[50] Xue W J, Miller O D. High-*NA* optical edge detection via optimized multilayer films[J]. Journal of Optics, 2021, 23(12): 125004.
[51] Doskolovich L L, Bykov D A, Bezus E A, et al. Spatial differentiation of optical beams using phase-shifted Bragg grating [J]. Optics Letters, 2014, 39(5): 1278-1281.
[52] Bykov D A, Doskolovich L L, Bezus E A, et al. Optical computation of the Laplace operator using phase-shifted Bragg grating[J]. Optics Express, 2014, 22(21): 25084-25092.
[53] Golovastikov N V, Bykov D A, Doskolovich L L, et al. Spatial optical integrator based on phase-shifted Bragg gratings[J]. Optics Communications, 2015, 338: 457-460.
[54] Golovastikov N V, Bykov D A, Doskolovich L L, et al. Analytical description of 3D optical pulse diffraction by a phase-shifted Bragg grating[J]. Optics Express, 2016, 24(17): 18828-18842.
[55] Wu W H, Jiang W, Yang J A, et al. Multilayered analog optical differentiating device: performance analysis on structural parameters[J]. Optics Letters, 2017, 42(24): 5270-5273.
[56] Zhou Y, Chen R, Chen W J, et al. Optical analog computing devices designed by deep neural network[J]. Optics Communications, 2020, 458: 124674.
[57] Zhou Y, Zhan J J, Chen R, et al. Analogue optical spatiotemporal differentiator[J]. Advanced Optical Materials, 2021, 9(10): 2002088.
[58] Liu Y, Huang M C, Chen Q K, et al. Single planar photonic chip with tailored angular transmission for multiple-order analog spatial differentiator[J]. Nature Communications, 2022, 13: 7944.
[59] Dai C J, Li Z, Shi Y Y, et al. Hydrogel-scalable nanoslide for switchable optical spatial-frequency processing[J]. Laser & Photonics Reviews, 2023, 17(4): 2200368.
[60] Wu Y L, Zhuang Z, Deng L, et al. Arbitrary multi-way parallel

mathematical operations based on planar discrete metamaterials [J]. Plasmonics, 2018, 13(2): 599-607.
[61] Chen C, Qi W, Yu Y, et al. On-chip optical spatial-domain integrator based on Fourier optics and metasurface[J]. Nanophotonics, 2021, 10(9): 2481-2486.
[62] Saba A, Tavakol M R, Karimi-Khoozani P, et al. Two-dimensional edge detection by guided mode resonant metasurface [J]. IEEE Photonics Technology Letters, 2018, 30(9): 853-856.
[63] Zhou Y, Wu W H, Chen R, et al. Analog optical spatial differentiators based on dielectric metasurfaces[J]. Advanced Optical Materials, 2020, 8(4): 1901523.
[64] Xu B Q, Huang G Q, Chen H C, et al. High-*NA* polarization-independent isotropic spatial differential metasurface[J]. Photonics and Nanostructures - Fundamentals and Applications, 2023, 53: 101107.
[65] Zhang W X, Zhang X D. Backscattering-immune computing of spatial differentiation by nonreciprocal plasmonics[J]. Physical Review Applied, 2019, 11(5): 054033.
[66] Hwang Y, Davis T J. Optical metasurfaces for subwavelength difference operations[J]. Applied Physics Letters, 2016, 109 (18): 181101.
[67] Hwang Y, Davis T J, Lin J A, et al. Plasmonic circuit for second-order spatial differentiation at the subwavelength scale[J]. Optics Express, 2018, 26(6): 7368-7375.
[68] Davis T J, Eftekhari F, Gómez D E, et al. Metasurfaces with asymmetric optical transfer functions for optical signal processing [J]. Physical Review Letters, 2019, 123(1): 013901.
[69] Zhang J H, Ruan Z C. Amplitude scaling and lateral shift of leaky radiation from surface plasmon excitation[J]. Journal of the Optical Society of America B, 2019, 36(2): 451-456.
[70] Pors A, Nielsen M G, Bozhevolnyi S I. Analog computing using reflective plasmonic metasurfaces[J]. Nano Letters, 2015, 15(1): 791-797.
[71] Doskolovich L L, Bezus E A, Bykov D A, et al. Spatial differentiation of Bloch surface wave beams using an on-chip phase-shifted Bragg grating[J]. Journal of Optics, 2016, 18(11): 115006.
[72] Zhang J, Zhou S, Dai X, et al. All-optical image edge detection based on the two-dimensional photonic spin Hall effect in anisotropic metamaterial[J]. Optics Express, 2023, 31(4): 6062-6075.
[73] Doskolovich L L, Bezus E A, Golovastikov N V, et al. Planar two-groove optical differentiator in a slab waveguide[J]. Optics Express, 2017, 25(19): 22328-22340.
[74] Dong Z W, Si J N, Yu X Y, et al. Optical spatial differentiator based on subwavelength high-contrast gratings[J]. Applied Physics Letters, 2018, 112(18): 181102.
[75] Bykov D A, Doskolovich L L, Morozov A A, et al. First-order optical spatial differentiator based on a guided-mode resonant grating[J]. Optics Express, 2018, 26(8): 10997-11006.
[76] Huang J Y, Zhang J H, Zhu T F, et al. Spatiotemporal differentiators generating optical vortices with transverse orbital angular momentum and detecting sharp change of pulse envelope [J]. Laser & Photonics Reviews, 2022, 16(5): 2100357.
[77] Long O Y, Guo C, Jin W L, et al. Polarization-independent isotropic nonlocal metasurfaces with wavelength-controlled functionality[J]. Physical Review Applied, 2022, 17(2): 024029.
[78] Wang H W, Guo C, Zhao Z X, et al. Compact incoherent image differentiation with nanophotonic structures[J]. ACS Photonics, 2020, 7(2): 338-343.
[79] Cotrufo M, Arora A, Singh S, et al. Dispersion engineered metasurfaces for broadband, high-*NA*, high-efficiency, dual-polarization analog image processing[EB/OL]. (2022-12-07) [2023-03-05]. https://arxiv.org/abs/2212.03468.
[80] Ruan Z C, Wu H, Qiu M, et al. Spatial control of surface plasmon polariton excitation at planar metal surface[J]. Optics Letters, 2014, 39(12): 3587-3590.
[81] Ruan Z C. Spatial mode control of surface plasmon polariton excitation with gain medium: from spatial differentiator to integrator[J]. Optics Letters, 2015, 40(4): 601-604.
[82] Zhang J H, Ying Q W, Ruan Z C. Time response of plasmonic spatial differentiators[J]. Optics Letters, 2019, 44(18): 4511-4514.
[83] Zhu T F, Zhou Y H, Lou Y J, et al. Plasmonic computing of spatial differentiation[J]. Nature Communications, 2017, 8: 15391.
[84] Fang Y S, Lou Y J, Ruan Z C. On-grating graphene surface plasmons enabling spatial differentiation in the terahertz region [J]. Optics Letters, 2017, 42(19): 3840-3843.
[85] Lou Y J, Fang Y S, Ruan Z C. Optical computation of divergence operation for vector fields[J]. Physical Review Applied, 2020, 14(3): 034013.
[86] Cordaro A, Kwon H, Sounas D, et al. High-index dielectric metasurfaces performing mathematical operations[J]. Nano Letters, 2019, 19(12): 8418-8423.
[87] Wan L, Pan D P, Yang S F, et al. Optical analog computing of spatial differentiation and edge detection with dielectric metasurfaces[J]. Optics Letters, 2020, 45(7): 2070-2073.
[88] Komar A, Aoni R A, Xu L, et al. Edge detection with Mie-resonant dielectric metasurfaces[J]. ACS Photonics, 2021, 8(3): 864-871.
[89] Golovastikov N V, Bykov D A, Doskolovich L L. Resonant diffraction gratings for spatial differentiation of optical beams[J]. Quantum Electronics, 2014, 44(10): 984-988.
[90] Golovastikov N V, Bykov D A, Doskolovich L L. Spatiotemporal pulse shaping using resonant diffraction gratings [J]. Optics Letters, 2015, 40(15): 3492-3495.
[91] Parthenopoulos A, Darki A A, Jeppesen B R, et al. Optical spatial differentiation with suspended subwavelength gratings[J]. Optics Express, 2021, 29(5): 6481-6494.
[92] Fang Y S, Ruan Z C. Optical spatial differentiator for a synthetic three-dimensional optical field[J]. Optics Letters, 2018, 43(23): 5893-5896.
[93] Lou Y J, Pan H, Zhu T F, et al. Spatial coupled-mode theory for surface plasmon polariton excitation at metallic gratings[J]. Journal of the Optical Society of America B, 2016, 33(5): 819-824.
[94] Rajabalipanah H, Momeni A, Rahmanzadeh M, et al. Parallel wave-based analog computing using metagratings[J]. Nanophotonics, 2022, 11(8): 1561-1571.
[95] Xu C Y, Wang Y L, Zhang C, et al. Optical spatiotemporal differentiator using a bilayer plasmonic grating[J]. Optics Letters, 2021, 46(17): 4418-4421.
[96] Bezus E A, Doskolovich L L, Bykov D A, et al. Spatial integration and differentiation of optical beams in a slab waveguide by a dielectric ridge supporting high-*Q* resonances[J]. Optics Express, 2018, 26(19): 25156-25165.
[97] Guo C, Xiao M, Minkov M, et al. Photonic crystal slab Laplace operator for image differentiation[J]. Optica, 2018, 5(3): 251-256.
[98] Guo C, Xiao M, Minkov M, et al. Isotropic wavevector domain image filters by a photonic crystal slab device[J]. Journal of the Optical Society of America A, 2018, 35(10): 1685-1691.
[99] Pan D P, Wan L, Ouyang M, et al. Laplace metasurfaces for optical analog computing based on quasi-bound states in the continuum[J]. Photonics Research, 2021, 9(9): 1758-1766.
[100] Zhou Y, Zheng H Y, Kravchenko I I, et al. Flat optics for image differentiation[J]. Nature Photonics, 2020, 14(5): 316-323.
[101] Malek S C, Overvig A C, Shrestha S, et al. Active nonlocal metasurfaces[J]. Nanophotonics, 2020, 10(1): 655-665.
[102] Kwon H, Sounas D, Cordaro A, et al. Nonlocal metasurfaces for optical signal processing[J]. Physical Review Letters, 2018, 121(17): 173004.

[103] Goh H, Alù A. Nonlocal scatterer for compact wave-based analog computing[J]. Physical Review Letters, 2022, 128(7): 073201.
[104] Ji A Q, Song J H, Li Q T, et al. Quantitative phase contrast imaging with a nonlocal angle-selective metasurface[J]. Nature Communications, 2022, 13: 7848.
[105] Kwon H, Cordaro A, Sounas D, et al. Dual-polarization analog 2D image processing with nonlocal metasurfaces[J]. ACS Photonics, 2020, 7(7): 1799-1805.
[106] Zangeneh-Nejad F, Khavasi A, Rejaei B. Analog optical computing by half-wavelength slabs[J]. Optics Communications, 2018, 407: 338-343.
[107] He S S, Zhou J X, Chen S Z, et al. Wavelength-independent optical fully differential operation based on the spin-orbit interaction of light[J]. APL Photonics, 2020, 5(3): 036105.
[108] Mi C Q, Song W Y, Cai X A, et al. Tunable optical spatial differentiation in the photonic spin Hall effect[J]. Optics Express, 2020, 28(20): 30222-30232.
[109] Xu W H, Ling X H, Xu D Y, et al. Enhanced optical spatial differential operations via strong spin-orbit interactions in an anisotropic epsilon-near-zero slab[J]. Physical Review A, 2021, 104(5): 053513.
[110] Xia D X, Wang Y, Zhi Q J. Tunable optical differential operation based on the cross-polarization effect at the optical interface[J]. Optics Express, 2021, 29(20): 31891-31901.
[111] Youssefi A, Zangeneh-Nejad F, Abdollahramezani S, et al. Analog computing by Brewster effect[J]. Optics Letters, 2016, 41(15): 3467-3470.
[112] Xu D Y, He S S, Zhou J X, et al. Optical analog computing of two-dimensional spatial differentiation based on the Brewster effect[J]. Optics Letters, 2020, 45(24): 6867-6870.
[113] Xu D Y, He S S, Zhou J X, et al. Goos-Hänchen effect enabled optical differential operation and image edge detection[J]. Applied Physics Letters, 2020, 116(21): 211103.
[114] Zhu T F, Lou Y J, Zhou Y H, et al. Generalized spatial differentiation from the spin Hall effect of light and its application in image processing of edge detection[J]. Physical Review Applied, 2019, 11(3): 034043.
[115] He S S, Zhou J X, Chen S Z, et al. Spatial differential operation and edge detection based on the geometric spin Hall effect of light [J]. Optics Letters, 2020, 45(4): 877-880.
[116] Wang R S, He S S, Luo H L. Photonic spin-Hall differential microscopy[J]. Physical Review Applied, 2022, 18(4): 044016.
[117] Ji Y W, Ma X K, Hu H J, et al. Enhanced edge detection based on spin Hall effect in the uniaxial crystal[J]. Frontiers in Physics, 2022, 10: 862156.
[118] Zhu T F, Huang J Y, Ruan Z C. Optical phase mining by adjustable spatial differentiator[J]. Advanced Photonics, 2020, 2 (1): 016001.
[119] Zhu T F, Guo C, Huang J Y, et al. Topological optical differentiator[J]. Nature Communications, 2021, 12: 680.
[120] Song B W, Wen S C, Shu W X. Topological differential microscopy based on the spin-orbit interaction of light in a natural crystal[J]. ACS Photonics, 2022, 9(12): 3987-3994.
[121] Wang Y, Yang Q, He S S, et al. Computing metasurfaces enabled broad-band vectorial differential interference contrast microscopy[J]. ACS Photonics, 2023, 10(7): 2201-2207.
[122] Wang R S, He S S, Chen S Z, et al. Computing metasurfaces enabled chiral edge image sensing[J]. iScience, 2022, 25(7): 104532.
[123] Li T, Yang Y, Liu X Y, et al. Enhanced optical edge detection based on a Pancharatnam-Berry flat lens with a large focal length [J]. Optics Letters, 2020, 45(13): 3681-3684.
[124] He Q, Zhang F, Pu M B, et al. Monolithic metasurface spatial differentiator enabled by asymmetric photonic spin-orbit interactions[J]. Nanophotonics, 2020, 10(1): 741-748.
[125] Xu D Y, Yang H A, Xu W H, et al. Inverse design of Pancharatnam-Berry phase metasurfaces for all-optical image edge detection[J]. Applied Physics Letters, 2022, 120(24): 241101.
[126] Zhou J X, Qian H L, Chen C F, et al. Optical edge detection based on high-efficiency dielectric metasurface[J]. Proceedings of the National Academy of Sciences of the United States of America, 2019, 116(23): 11137-11140.
[127] Zong M X, Liu Y Q, Lü J W, et al. Two-dimensional optical differentiator for broadband edge detection based on dielectric metasurface[J]. Optics Letters, 2023, 48(7): 1902-1905.
[128] Huo P C, Zhang C, Zhu W Q, et al. Photonic spin-multiplexing metasurface for switchable spiral phase contrast imaging[J]. Nano Letters, 2020, 20(4): 2791-2798.
[129] Kim Y J, Lee G Y, Sung J W, et al. Spiral metalens for phase contrast imaging[J]. Advanced Functional Materials, 2022, 32 (5): 2106050.
[130] Zhou J X, Qian H L, Zhao J X, et al. Two-dimensional optical spatial differentiation and high-contrast imaging[J]. National Science Review, 2021, 8(6): nwaa176.
[131] Fu W W, Zhao D, Li Z Q, et al. Ultracompact meta-imagers for arbitrary all-optical convolution[J]. Light: Science & Applications, 2022, 11: 62.
[132] Wesemann L, Rickett J, Song J C, et al. Nanophotonics enhanced coverslip for phase imaging in biology[J]. Light: Science & Applications, 2021, 10: 98.
[133] Zhang Y Z, Lin P C, Huo P C, et al. Dielectric metasurface for synchronously spiral phase contrast and bright-field imaging[J]. Nano Letters, 2023, 23(7): 2991-2997.

Development and Applications of Spatial Optical Analog Computing

Liu Yongliang[1], Liu Wenwei[1], Cheng Hua[1*], Chen Shuqi[1,2,3**]

[1]*The Key Laboratory of Weak Light Nonlinear Photonics, Ministry of Education, TEDA Institute of Applied Physics, School of Physics, Nankai University, Tianjin* 300071, *China*;

[2]*Smart Sensing Interdisciplinary Science Center, School of Materials Science and Engineering, Nankai University, Tianjin* 300350, *China*;

[3]*Collaborative Innovation Center of Extreme Optics, Shanxi University, Taiyuan* 030006, *Shanxi*, *China*

Abstract

Significance The rapid development in fields such as artificial intelligence, autonomous driving, and big data has brought higher demands for computational tools due to the massive amount of data involved. In recent years, with the development of ultra-large-scale integrated circuits, the volume of electronic computers has been significantly reduced, and the data processing speed has been greatly improved. However, electronic devices are gradually constrained by physical limitations such as quantum effects, which slow down the improvement speed of low-power and miniaturized digital computing circuits. In addition, traditional analog signal processing requires processes such as analog-to-digital conversion, signal processing units, and digital-to-analog conversion. The inevitable conversion delays and high-power consumption of electronic devices make traditional analog computing incapable of large-scale information processing. Therefore, researchers are devoted to developing new computing systems to overcome the limitations of traditional electronic computing systems. One of the technologies that has attracted significant attention is the construction of all-optical systems for information transmission and processing using optical signals as carriers.

Optical information processing technology has attracted increasing attention due to its advantages such as ultra-high speed, large bandwidth, and low loss. People have attempted to introduce optical methods to improve the performance of information processing and have successfully designed various optical analog computing devices. Compared with electronic signal processing systems, optical signal processing can be categorized into digital computing and analog computing. The earliest digital computing of optical signals uses a liquid crystal spatial light modulator based on optoelectronic mixing for logical operations. Optical analog computing does not involve optoelectronic conversion and can directly manipulate optical signals in time and space domains. Due to the parallelism of physical processes such as light field promotion and interference in space, spatial optical analog computing offers advantages in information processing such as ultra-fast speed, high throughput, and low energy consumption. These attributes highlight its significant potential for applications in image processing, edge detection, and machine learning.

Progress Traditional spatial optical analog operations often employ the Fourier optical 4*f* system, which involves components such as lenses and filters. However, in recent years, the rapid development of micro-nano optics and fabrication processes has made it possible to realize spatial analog computing using devices at sub-wavelength scales. This opens up possibilities for miniaturization, on-chip integration, and integration of optical computing systems. At present, research on spatial optical analog computing primarily focuses on achieving spatial differentiation, integration, and equation solving. The main design principles can be classified into three categories: effective medium theory, resonance principle, and non-resonance principle (Fig. 1). Spatial analog computing can be achieved by integrating metasurfaces and GRIN lenses into a 4*f* system. By designing the spatial distribution of transmission (or reflection) rates of the metasurface, researchers can obtain the spatial spectral transfer function for the desired mathematical operations. However, this method requires the introduction of spatial Fourier transform and inverse Fourier transform, resulting in larger device dimensions. Another approach involves constructing a multilayer flat-stack structure using multiple materials, where various spatial optical analog computations can be achieved by adjusting the refractive index and thickness parameters of each layer (Fig. 2). Devices designed based on the equivalent medium theory have complex structures and pose challenges in practical fabrication. In a resonant system, the excitation of resonance requires momentum matching, which leads to different responses of the resonant structure to wavevector components in different directions of the incident light. This allows the spatial response of the propagating optical field in the structure to conform to specific optical simulation operations at certain frequencies, without the need for Fourier transform (Fig. 3). In contrast to the limited spatial bandwidth of resonant-based analog devices, under specific conditions in non-resonant systems, researchers can obtain the spatial spectral transfer function required for spatial analog operations based on the spin Hall effect, Brewster effect, and PB phase (Fig. 4). Spatial optical analog computing enables high-speed, high-throughput, and low-power information

processing. Spatial differentiation and convolution operations can be directly applied to image edge detection and are promising for applications in pattern recognition, machine vision, and other fields (Fig. 5). Finally, the existing challenges and research prospects of spatial optical analog computing are discussed.

Conclusions and Prospects We summarize the development of optical spatial analog computing and focus on the research progress and applications of optical spatial analog computing with metasurfaces in different theoretical models and systems. By incorporating artificial nanostructures to replace conventional large-scale optical components, metasurfaces enable the development of miniaturization and integration of spatial optical analog computing devices. Furthermore, we analyze the latest advances in spatial optical analog computing based on physical effects such as spin-orbit coupling and topology, which present novel avenues for achieving ultra-wideband and high-speed information processing. Lastly, we discuss the existing challenges and research prospects associated with optical spatial analog computing, shedding light on future directions for this field. With the development of information technology and the increasing demand for processing performance, optical information processing methods are gradually emerging. The design and implementation of various optical analog computing devices have become increasingly important for technological development and performance improvement. Spatial optical analog computing combined with metasurfaces has made unexpected progress, but it still suffers from some challenges such as the fabrication technology of metasurfaces, energy efficiency of optical analog computing, and reconfigurable computing. In the future, spatial analog computing combined with metasurfaces will unveil more innovative approaches, promoting the development of spatial analog computing from simple to complex. With continuous innovative advances in technology, combining various computing devices and achieving multi-functional optical computing chips may further boost fields such as high-throughput optical communication and optical imaging in the future.

Key words spatial optical analog computing; spatial differentiators; Fourier optics; metasurface; spin Hall effect of light